Analysis of a Novel Double-Barreled Anion Channel from Rat Liver Rough Endoplasmic Reticulum

Nicole Morier and Rémy Sauvé
Groupe de recherche en transport membranaire, Département de physiologie, Université de Montréal, Québec H3C 3J7, Canada

ABSTRACT The presence of anionic channels in stripped rough endoplasmic reticulum membranes isolated from rat hepatocytes was investigated by fusing microsomes from these membranes to a planar lipid bilayer. Several types of anion-selective channels were observed including a voltage-gated Cl^- channel, the activity of which appeared in bursts characterized by transitions among three distinct conductance levels of 0 pS (0 level), 160 pS (O_1 level), and 320 pS (O_2 level), respectively, in 450 mM (*cis*) 50 mM (*trans*) KCl conditions. A χ^2 analysis on current records where interburst silent periods were omitted showed that the relative probability of current levels 0 (baseline), O_1, and O_2 followed a binomial statistic. However, measurements of the conditional probabilities W(level 0 at τ/level O_2 at 0) and W(level O_2 at τ/level 0 at 0) provided clear evidence of direct transitions between the current levels 0 and O_2 without any detectable transitions to the intermediate level O_1. It was concluded on the basis of these results that the observed channel was controlled by at least two distinct gating processes, namely 1) a voltage-dependent activation mechanism in which the entire system behaves as two independent monomeric channels of 160 pS with each channel characterized by a simple Open-Closed kinetic, and 2) a slow voltage-dependent process that accounts for both the appearance of silent periods between bursts of channel activity and the transitions between the current levels 0 and O_2. Finally, an analysis of the relative probability for the system to be in levels 0, O_1, and O_2 showed that our results are more compatible with a model in which all the states resulting from the superposition of the two independent monomeric channels have access at different rates to a common inactivated state than with a model where a simple Open-Closed main gate either occludes or exposes simultaneously two independent 160-pS monomers.

INTRODUCTION

Several studies have indicated that the release and/or uptake of Ca^{2+} and H^+ ions in intracellular stores is compensated for by an opposite charge movement to maintain electroneutrality (Bayerdörffer et al., 1984; Muallem et al., 1985; Kemmer et al., 1987; Shah et al., 1987, 1988; Palade et al., 1989). For instance, there is evidence that the Ca^{2+} uptake in rough endoplasmic reticulum (RER) vesicles varies according to the monovalent cations and anions present in the extravesicular medium (Bayerdörffer et al., 1984; Kemmer et al., 1987). Despite these observations, the exact nature of the ionic pathways involved in counter-ion movement remains still poorly circumscribed. Several reports have suggested the implication of Cl^- selective channels. For example, two different anion channels have been identified in endoplasmic reticulum (ER) vesicles from rat exocrine pancreas (Schmid et al., 1988). They are a Cl^- channel of large conductance (260 pS in 140 mM KCl) strongly regulated by voltage, and a voltage-insensitive channel also permeable to Cl^- ions but of smaller unitary conductance (79 pS). The presence of anion channels in giant liposomes prepared from rat liver ER vesicles was also reported by Keller et al. (1988) in an abstract. More recently, Murray and Ashley (1991) have identified an intracellular anion channel from rat microsomes that is also permeable to cations. It is generally assumed that these anion channels are involved in the maintenance of electroneutrality during Ca^{2+} uptake in the RER. Finally, large aqueous channels in membrane vesicles derived from the RER of canine pancreas were recorded by Simon et al. (1989). Conductances of 20, 55, 80, and 115 pS in 450 mM K^+-glutamate were observed, but it was not established whether these different conductances represent distinct channels or subconductances of a single channel-forming protein.

Anion selective channels have been studied more extensively in sarcoplasmic reticulum (SR) membrane preparations. For instance, Hals et al. (1989) have identified a Cl^- selective channel of large conductance (505 pS in 200 mM Cl^-) using the patch clamp technique on "sarcoball" preparations from frog skeletal muscles. Single channel recordings of voltage-dependent Cl^- channels were also obtained by fusion to a planar lipid bilayer of membrane vesicles isolated from mammalian skeletal (Tanifuji et al., 1987; Rousseau et al., 1988) or cardiac muscles (Rousseau, 1989). Although the physiological role of these channels remains to be confirmed, a counter-ion function associated with Ca^{2+} release and/or reuptake has been often proposed.

We have investigated the presence of anionic channels in stripped rough endoplasmic reticulum (SRER) membranes from rat hepatocytes by the technique of fusion of SRER microsomes to a planar lipid bilayer. These experiments have led to the identification of a voltage-regulated double-barreled Cl^- channel of 160 pS in 450 mM KCl. The gating properties of this channel are similar to those found by Miller and co-workers for the double-barreled chloride channel in the *Torpedo californica* electroplax surface membrane (see Miller, 1982; Hanke and Miller, 1983). However, the two

Received for publication 14 September 1993 and in final form 19 May 1994.
Address reprint requests to Dr. Rémy Sauvé, Département de physiologie, Université de Montreal, C. P. 6128, Succ. Centre-ville, Montreal, Québec H3C 3J7. Tel.: 514-343-5813 or 6111, ext. 3295; Fax: 514-343-2111.

0006-3495/94/08/590/13 $2.00

channels differ in terms of their respective unitary conductance and in the voltage dependence of the gating processes responsible for channel activation and inactivation. A preliminary account of this work has appeared already (Morier and Sauvé, 1993).

MATERIALS AND METHODS

Materials

Natural L-α-phosphatidylglycerol (PG) of egg was obtained from Avanti Polar Lipids (Birmingham, AL). GTP and squalene were purchased from Sigma Chemical Co. (St. Louis, MO) and *n*-decane from Fisher Scientific (Pittsburgh, PA). GTP was received on dry ice and stored at −80°C. Salts, reagents, and solvent were analytical grade. Salt solutions were filtered through microfilters with a pore size of 0.2 μm (Millipore Corporation, Boston, MA).

Preparation of microsomal membrane vesicles

Subcellular fractions were prepared from rat liver homogenates according to the procedure of Paiement and Bergeron (1983). All steps were performed at 4°C. Briefly, liver tissue from three male Sprague-Dawley rats (225–250 g each) that had fasted overnight was homogenized in a medium containing 250 mM sucrose (40% w/v) with 20 strokes of a motor-driven Teflon pestle and filtered through nylon mesh of 150 μm. The homogenate was centrifuged at 8700 × *g* (Beckman J 20, Beckman Instruments, Inc., Porterville, CA) for 25 min, the pellet discarded, and the supernatant centrifuged at 43,000 × *g* (Beckman Ti 60) for 13 min. The supernatant with a small part of the pellet was centrifuged at 110,000 × *g* (Beckman Ti 60) for 1 h.

Subfractionation of the crude microsome preparation was performed on a discontinuous sucrose gradient (0.25 M, 0.86 M, and 1.0 M); 1.4 ml of the crude microsome suspension at 1.38 M sucrose was overlayered on a 2.5-ml sucrose gradient. Gradients were centrifuged at 300,000 × *g* (Beckman SW 60) for 1 h. The resulting pellet, which contained predominantly RER, was resuspended in a solution containing 250 mM sucrose and 3 mM imidazole at pH 7.4. Rough microsomes were stripped of ribosomes by treatment with sodium pyrophosphate 0.5 mM (25% v/v). After incubation on ice for 15 min, microsomes were pelleted by centrifugation at 140,000 × *g* (Beckman Ti 50) for 40 min, resuspended in sucrose-imidazole buffer at pH 7.4, and washed twice with a sucrose-imidazole buffer. At the end, the rough microsome pellet was suspended in 250 mM sucrose-imidazole at a final concentration of 8–9 mg of protein/ml and stored at −80°C until they were used. Protein concentration was measured using bovine serum albumine (25 mg/ml) as standard.

Characterization of rough microsomal membrane vesicles

The stripped rough microsome (SRM) membranes used for channel incorporation have already been characterized by Paiement et al. (1987). These microsomal fractions of ER retained their protein synthesis activity and were oriented in the right-side-out configuration (Paiement et al., 1988).

Planar lipid bilayers formation

Single channel measurements were carried out using the so-called chamber partition technique. Black lipid membranes (BLM) were formed at room temperature from a suspension of PG in decane at a final concentration of 25 mg/ml. The BLM was painted over a 200 μm-diameter aperture drilled in a Delrin partition, which separated two chambers containing, respectively, 3 (*cis*) and 5 (*trans*) ml of solution. The outline of the aperture was coated with squalene before the application of the lipid suspension.

Rough microsome vesicles fusion

Conventional fusion techniques (osmotic gradients, divalent cation (Ca^{2+}) plus negatively charged bilayers) were for the most part ineffective at promoting fusion of SRER microsomes to BLM (see also Schmid et al., 1988). However, a report by Paiement et al. (1987) indicated that the fusion of SRM was stimulated in the presence of GTP and divalent cations such as Mn^{2+} and Mg^{2+}. Furthermore, preliminary experiments showed that exogenous PG liposomes facilitated the fusion of membrane vesicles (J. Paiement, personal communication). Our approach consisted therefore of adding GTP (0.5 mM) to the chamber (*cis*) where the vesicles were injected and using planar BLM formed of PG in decane (Paiement et al., 1987). We found that the presence of GTP increased the probability of fusion without being essential to the fusion process. In addition, GTP could not be replaced by other nucleotides. Neither ATP, ADP, CTP, ITP, UTP, GDP, nor nonhydrolyzable GTP analogues in concentrations ranging from 0.1–1 mM were as effective as GTP in promoting fusion. The bilayers were first bathed in symmetrical solutions containing (in mM): 50 KCl, 7.5 $MgCl_2$, and 2.5 $MnCl_2$, buffered with 10 mM TRIS/HCL, pH 7.4. After membrane formation, the concentration of KCl in the *cis* chamber was increased to 450 mM by adding 400 μl of a 3-M KCl stock solution. Aliquots of membranes vesicles (≈180 μg protein) were injected close to the bilayer in the compartment referred as the *cis* chamber. Under these conditions, single channel activity was still observed in less than 5% of bilayers formed.

Data acquisition and analysis

Single channel currents were measured by means of a custom-made I-V converter (Sauvé et al., 1983). The voltage was applied to the *trans* chamber through $Ag/AgCl_2$ electrodes connected to high-salt (KCl, 3M) agar bridges with the *cis* chamber held at ground. Junction potentials (<3 mV) were measured and corrected before each experiment. The signals were stored on videotapes (SONY, SL-300) and subsequently transferred in continuous mode to a hard disk at a sampling rate ranging from 3 to 30 kHz. Unless specified otherwise, low-pass filtration of the stored signals was performed using two four-pole Bessel filters connected in series with cutoff frequencies corresponding to the selected sampling rate/5.0. The unitary current amplitudes were derived from amplitude histograms as described elsewhere (Sauvé et al., 1986). For χ^2 analysis, current amplitude intervals were first selected from a current amplitude histogram in which all the values of a digitized current record were considered. These intervals were used to define a series of current classes corresponding respectively to no channel open, one channel open, etc., up to N channels open simultaneously, where N is the total number of channels detected. A second amplitude histogram, in which a limited small number (500), N_r, of independent current values were classified according to the current classes defined in the first histogram, was then computed from the same current record. The resulting numbers were finally compared with a binomial distribution of the form

$$P(N, r) = \frac{N!\, P_o^r (1 - P_o)^{N-r}}{r!\,(N - r)!} \tag{1}$$

where $P(N, r)$ represents the probability of having r channels open among N with P_o given by

$$P_o = \frac{\sum_{r=1}^{N} rP(N, r)}{N} \tag{2}$$

The χ^2 values were computed according to

$$\chi^2 = \frac{\sum_{r=0}^{N} (N_r - N_t P(N, r))^2}{N_r} \tag{3}$$

where N_r is the number of observed independent current values in the rth current class (r channels open simultaneously). The number of degrees of freedom was taken as N.

Time-interval distributions were measured on noise-free Markov signals created from experimental current records according to Baum-Welch re-estimation formulae described by Chung et al. (1990). The Hidden Markov Models (HMM) procedure was usually applied on successive segments of

200,000 samples and included a minimum of seven states corresponding to different current levels. The current level associated with each state and the transition rates between connected states were both adjusted so as to maximize the likelihood that the proposed kinetic scheme accounts point by point for the entire digitized current record. This approach led to the selection of 50% threshold current values that prevented systematically the detection of transitions to current levels with a low probability of occurrence (less than 0.01).

Finally, transition rates between current levels were estimated using two different procedures. The first approach consisted of measuring $W_s(i, \tau/j, 0)$, the conditional probability that the system be in state i at τ knowing that it was in state j at 0. $W_s(i, \tau/j, 0)$ was computed from the ratio

$$W_s(i, \tau/j, 0) = \frac{W_o((i, \tau), (j, 0))}{P_s(j, 0)} \tag{4}$$

where $W_o((i, \tau),(j, 0))$ = Probability (of the system being in state i at τ and in state j at 0) and $P_s(j, 0)$ = Probability (of the system being in state j at 0).

The conditional probability matrix W_s is the solution of the Kolmogorov forward differential equation, namely,

$$\frac{dW_s}{dt} = QW_s \tag{5}$$

where Q is the microscopic generator matrix with $Q_{i,j}$ the transition rate from state j to state i and

$$Q_{i,i} = -\sum_{l \neq i}^{n_s} Q_{l,i} \tag{6}$$

where n_s is the number of states. The formal solution for W_s is given by

$$W_s = \exp(Qt) = I + Qt + \frac{(Qt)^2}{2} + \frac{(Qt)^3}{3!} + \cdots \tag{7}$$

where I is the identity matrix. The conditional probability $W_s(i, \tau/j, 0)$ can thus be expressed as a power series of τ such that

$$W_s(i, \tau/j, 0) = (Q_{i,j})\,\tau + \alpha_2\tau^2 + \alpha_3\tau^3 + \cdots \tag{7a}$$

where the coefficients α_i $i \geq 2$ are expressions that take into account transitions from state j to state i through intermediate states. The transition rate from state j to i can be therefore estimated directly by measuring $W_s(i, \tau/j, 0)$ for values of τ much smaller than the characteristic time of correlation between these two states. Several states may lead, however, to the same current level. Let level (k) with $1 \leq k \leq n_s$ be the current level associated with state k, and $L_1, L_2, L_3 \cdots, L_{nl}$ be the current levels observed experimentally. Under these conditions, the conditional probability that the system be in current level L_i at τ given that it was in current level L_j at 0, $W(L_j, \tau/L_j, 0)$, reads

$$W(L_i, \tau/L_j, 0) = \sum_{m=1}^{n_s} \sum_{l=1}^{n_s} W_s(l, \tau/m, 0)\, \delta_{\text{level}(m),L_j}\, \delta_{\text{level}(l),L_i} \tag{8}$$

with

$$\delta_{\text{level}(m),L_j} = 0 \quad \text{if level (m)} \neq L_j \quad \text{and} \quad \delta_{\text{level}(l),L_i} = 0 \quad \text{if level (l)} \neq L_i$$

$$\delta_{\text{level}(m),L_j} = 1 \quad \text{if level (m)} = L_j \quad \text{and} \quad \delta_{\text{level}(l),L_i} = 1 \quad \text{if level (l)} = L_i$$

From Eqs. 7a and 8 it follows that

$$W(L_i, \tau/L_j, 0) = \left(\sum_{m=1}^{n_s} \sum_{l=1}^{n_s} Q_{l,m}\, \delta_{\text{level}(m),L_j}\, \delta_{\text{level}(l),L_i} \right) \tau + \beta_1\tau^2 + \beta_2\tau^3 + \cdots . \tag{9}$$

On the basis of Eq. 9, the power series expansion of $W(L_i, \tau/L_j, 0)$ will not contain a linear term in τ if there are no direct transitions from L_j to L_i. However, higher-order terms may be present, because of transitions from L_j to L_i via intermediate current levels. By curve fitting to a polynomial function the values of $W(L_i, \tau/L_j, 0)$ measured experimentally at various τ values, it is thus possible to provide a clear indication of direct transitions between two selected current levels and estimate the rate at which these transitions take place. An example of conditional probability analysis is presented in Appendix 1.

Transition rates between current levels were also measured using the HMM method described previously. This method was found, however, to often introduce pseudo-intermediate current levels as a way to account for the effect of filtering on current transitions. This was particularly important in current records digitized at a high frequency. The conditional probability procedure was less sensitive to filtering mainly because the experimental values of $W(L_i, \tau/L_j, 0)$ were derived over time intervals much longer that the characteristic time response of the filters (0.1–0.3 ms). Both methods yielded nevertheless the same transition rates in most cases.

RESULTS

Incorporation experiments led to the identification of at least three different types of anion-selective and two different types of K^+-permeable channels. Fig. 1 illustrates an example of a series of single channel recordings obtained at various holding potentials after the fusion of microsomal SRER vesicles in 450 mM (*cis*) ‖ 50 mM (*trans*) KCl conditions. Downward current jumps corresponding to channel openings were observed at voltages ranging from −35 to +30 mV. At potentials more negative than −35 mV, current jumps could not be resolved unambiguously. Clearly, the current jump amplitude increased as more positive *trans* potentials were applied. In addition, the channels obtained by incorporation showed a voltage-dependent fluctuation pattern characterized at positive potentials by the appearance of bursts of channel openings separated by long silent periods, the duration of which increased at positive potential values. Similar current fluctuations were observed in 25% of the experiments performed on 12 different vesicle preparations. However, most of these experiments led to multiple channel recordings with more than one channel of the same type present or with at least two different channel types. Two

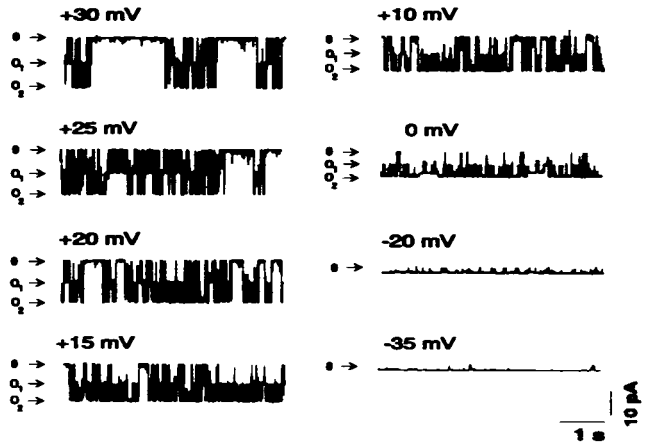

FIGURE 1 Single channel activity. Single channel activity recorded after fusion of SRER microsomes to a PG planar bilayer in asymmetrical 450 mM (*cis*) ‖ 50 mM (*trans*) KCl conditions. Both KCl solutions contained in addition (in mM): 7.5 $MgCl_2$ and 2.5 $MnCl_2$ buffered at pH 7.4 with 10 mM TRIS/HCl. Recordings filtered at 500 Hz. Current levels are identified as levels 0, O_1 and O_2.

experiments only, each one from a different membrane preparation, yielded recordings with a single functional channel and could thus be used for a detailed analysis at the single-channel level of the channel-gating processes. Fig. 2 shows the current amplitude probability density plotted as a function of current amplitude for various potentials. Three distinct current levels are apparent, suggesting either the presence of at least two functional channels or a single channel characterized by two subconducting states. The resulting current-voltage relationship associated with each of these current levels is shown in Fig. 3. The curves are linear for voltages ranging from −20 to +45 mV, and the extrapolated reversal potential is clearly more negative than −35 mV in both cases, indicating on the basis of the Goldmann-Hodgkin-Katz equation a permeability ratio P_{Cl}/P_K greater than 7.2. A linear regression analysis of curves A and B led to inward current conductances of 160 ± 2 and 320 ± 2 pS (n = 5), respectively. Therefore, the current records in Fig. 1 are representative of either two channels of equal conductance or a single channel with two substates of identical conductance value.

Binomial analysis

To test the hypothesis that the current amplitude histograms shown in Fig. 2 correspond to a binomial distribution of two independent channels, a χ^2 analysis on 500 independent observations was undertaken as described in Materials and Methods. The results presented in Table 1 clearly indicate that the current amplitude histograms obtained at positive voltages were not compatible with this hypothesis for a confidence coefficient set to 0.95 (χ^2 = 6.28 for 2 degrees of freedom). However, a significant agreement between experimental and theoretical values was obtained at 0, −10, and

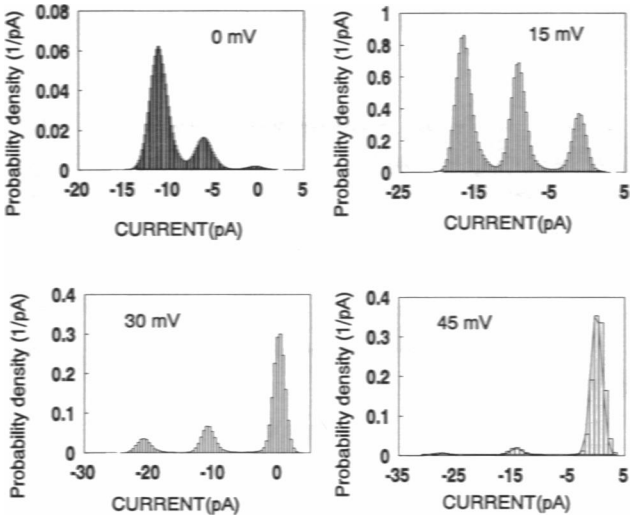

FIGURE 2 Current probability density as a function of current amplitude. Current probability density as a function of current amplitude measured at four different potentials. The probability of occurrence of a given current level was determined by numerically integrating the probability density function over the current amplitude interval associated with that level.

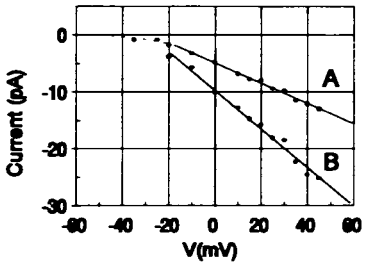

FIGURE 3 I/V relationships. Current amplitudes were estimated from current amplitude histograms obtained from single channel records measured at various applied voltages. The amplitude of both current levels showed a linear relation as a function of voltage (*trans* relative to *cis*) with slope conductances of 160 ± 2 pS (*A*) and 320 pS ± 2 (*B*) respectively (n = 5). The 0 current potential is clearly <−35 mV (see above) indicating a channel with a permeability ratio P_{Cl}/P_K > 7.2.

TABLE 1 χ^2 analysis performed on nonsegmented current records

Voltage, mV	State	Experimental Observation	P_o	Theoretical Prediction	χ^2
	0	419		408	
+45	1	65	0.10	88	22.5
	2	16		5	
	0	345		320	
+30	1	105	0.20	160	58.2
	2	49		21	
	0	218		122	
+25	1	154	0.50	250	75.6
	2	128		128	
	0	148		119	
+20	1	190	0.51	250	20.3
	2	161		131	
	0	93		50	
+15	1	174	0.68	216	45.1
	2	234		234	
	0	94		30	
+10	1	121	0.75	185	158.7
	2	284		285	
	0	9		8	
0	1	114	0.88	113	0.14
	2	376		378	
	0	7		3	
−10	1	62	0.93	66	5.5
	2	431		431	
	0	1		1	
−20	1	27	0.97	27	0.0
	2	472		472	

The probability of occurrence at a given potential for each current level (0, O_1, and O_2) was computed from the current amplitude histogram derived from 500 independent current values as described in Materials and Methods. The theoretical binomial distribution was estimated with P_o calculated according to Eq. 2. The test statistic corresponded to χ^2 as defined in Eq. 3, and to reject the hypothesis of a binomial distribution the value of this statistic had to be larger than $\chi^2_{.05}$ = 6.28 (based on 2 degrees of freedom).

−20 mV. On the basis of this result, it can be concluded that the current fluctuations recorded at positive *trans* potentials cannot be described in terms of two independent identical channels. The nonbinomial distribution of the current levels at positive potentials may have resulted, however, from the

TABLE 2 χ^2 analysis performed on segmented current records

Voltage, mV (N_r)	State	Experimental Observation	P_o	Theoretical Prediction	χ^2
	0	180		182	
+45	1	245	0.40	240	0.24
(500)	2	75		78	
	0	91		97	
+30	1	254	0.55	242	1.20
(490)	2	145		151	
	0	77		70	
+25	1	217	0.62	229	1.52
(488)	2	195		189	
	0	65		61	
+20	1	215	0.65	225	0.94
(497)	2	217		210	
	0	35		39	
+15	1	205	0.72	201	0.49
(500)	2	260		260	
	0	28		23	
+10	1	156	0.79	167	1.89
(500)	2	316		311	

The probability of occurrence at a given potential for each current level (0, O_1, and O_2) was computed from a current amplitude histogram derived from 500 independent current values selected from current records in which the interburst silent periods were omitted. The theoretical binomial distribution was estimated with the value of P_o calculated according to Eq. 2. The χ^2 analysis was carried out as described in Table 1. The numbers in parentheses indicate N_r.

presence of long silent periods between bursts of openings. This hypothesis was tested in a second χ^2 analysis where silent periods between bursts of activity were systematically omitted. The results are presented in Table 2. This segmentation procedure led to current amplitude histograms that were now compatible with the predictions of a binomial distribution with a confidence coefficient of 0.95. This analysis would therefore support the proposal of a channel activation mechanism in which the entire system behaves within each

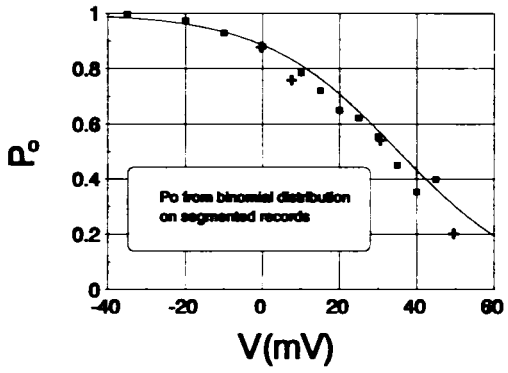

FIGURE 4 Voltage dependence of the open probability for a single monomeric channel. Open probability computed using Eq. 2 on current records obtained from two independent vesicle preparations. Interburst silent periods were omitted in each case to ensure that the current level distribution followed a binomial statistic as shown in Table 2.

individual burst of channel activity, as two independent monomeric channels. Fig. 4 presents the change in open probability for a single monomeric channel as a function of the applied voltage for current records coming from two independent series of experiments. The open probability was computed according to Eq. 2 on current records in which silent interburst periods were omitted. The results illustrated in Fig. 4 show that the open probability of each monomeric channel decreased at increasing *trans* potential values.

Voltage dependence of the transition rates

Despite the evidence that the distribution of the current levels within individual current bursts or in current records measured at negative potentials followed a binomial statistic, a large number of transitions were observed that could not be explained assuming two independent 160-pS channels. Fig. 5 shows an example of current traces, in which current tran-

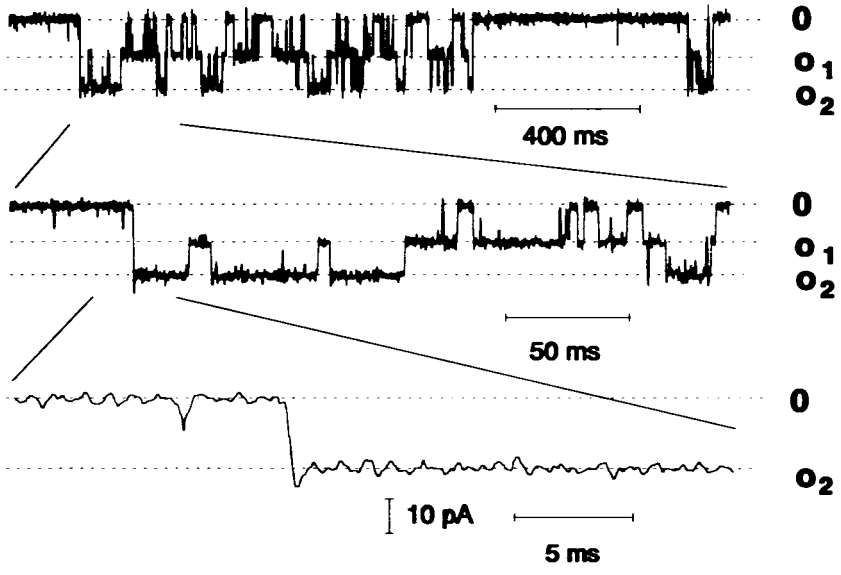

FIGURE 5 Direct transitions between current levels O_2 and 0. Example of current transitions among three different current levels recorded at +30 mV at different time scales. The level 0 corresponds to the current level when no channel is open. The current levels marked O_1 and O_2 indicate the opening of one or two monomeric channels, respectively. *Bottom:* Evidence of direct transitions occurring between levels 0 and O_2 without any detectable intermediate transitions to level O_1. Original record filtered at 5 kHz and sampled at 30 kHz.

sitions occurred directly from the maximum current level (O_2 level) to the baseline (O level) and vice versa without any detectable transition to the intermediate current value (O_1 level). Such behavior is not expected for a system in which all the transitions arise from the openings and/or closings of two identical monomeric channels. In fact, a binomial system would predict that transitions from level O_2 to level 0 necessarily involve transitions to the intermediate O_1 level. The occurrence of direct transitions between levels 0 and O_2 was thus investigated using the conditional probability approach described in Materials and Methods. Fig. 6 *A* shows the time dependence of the conditional probability *W* (level 0, τ/level O_2, 0) measured from current traces recorded at 0 (▲), 15 (◆), 30 (■), and 45 mV (●) as a function of τ. The continuous lines represent the results obtained by curve fitting each set of experimental data to a polynomial function of the form $\alpha_1\tau + \alpha_2\tau^2 + \alpha_3\tau^3$. An important linear component, $\alpha_1\tau$, was estimated in each case, thus providing support for direct transitions from level O_2 to level 0 without transitions to the intermediate O_1 level. In addition, the contribution of the linear coefficient α_1 did not change significantly using higher-order polynomial functions, the contribution of the cubic term $\alpha_3\tau^3$ accounting usually for less than 5% of $\alpha_1\tau$ for values of τ less than 5 ms. In Fig. 6 *B* the transition rates from level 0 to level O_2 and from level O_2 to level 0 are plotted on a semilogarithm scale. These rates correspond to the coefficients α_1 estimated by curve fitting, respectively, the conditional probability *W*(level 0, τ/level O_2, 0) and *W*(level O_2, τ/level 0, 0) (see Materials and Methods). The results in Fig. 6 *B* clearly indicate that the transition rates from level 0 to level O_2 and from level O_2 to level 0 depend on voltage as single exponential functions. The continuous lines were calculated using

$$\text{Rate from level } O_2 \text{ to level } 0 = 0.55e^{[1.97\ qV/KT]} \quad (10)$$

and

$$\text{Rate from level } 0 \text{ to level } O_2 = 29e^{[-2.74\ qV/KT]} \quad (11)$$

where *V* is the applied voltage in mV; *q*, the electronic charge; *K*, Boltzman's constant; and *T*, the absolute temperature. A variation of 12.7 mV will thus lead to an *e*-fold change in the transition rate from level O_2 to level 0, whereas a 9-mV increase will cause an *e*-fold decrease in the transition rate from level 0 to level O_2. It is likely that the transitions from level O_2 to level 0 account for the appearance of bursts of channel activity as illustrated in Fig. 1. This would explain the absence of clear current bursts at negative potentials, the number of transitions from level O_2 to level 0 decreasing sharply as the potential becomes more negative.

Transition rates from level O_1 to O_2 and from level O_2 to O_1 were also computed using the conditional probability procedure illustrated in Fig. 6 *A*. Fig. 7 *A* shows an example of conditional probability analysis for current transitions from level O_1 to O_2. The continuous lines represent the predictions of a polynomial fit procedure using functions of the form $\alpha_1\tau + \alpha_2\tau^2 + \alpha_3\tau^3$ as described previously. Fig. 7 *B* presents the transition rates from level O_1 to O_2 and from level O_2 to O_1 as a function of voltage. The transition rates were derived either from the coefficient α_1 obtained by curve fitting the data points illustrated in Fig. 7 *A* (*circles*, *squares*) or by using the HMM computational algorithm (*diamonds*, *triangles*) as described in Materials and Methods. In the latter case best results were achieved starting with the following HMM eight-state model:

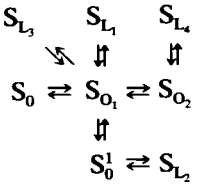

It must be pointed out, however, that the current levels assigned to S_0^1 and S_0 were set equal to ensure that the model properly accounts for the long silent periods between bursts of channel activity. In addition, direct transitions between levels O_2 and 0 were not included so as to prevent the introduction by the HMM algorithm of intermediate pseudo-current levels resulting from the finite rise time of the current transitions caused by filtering. An example of HMM signal

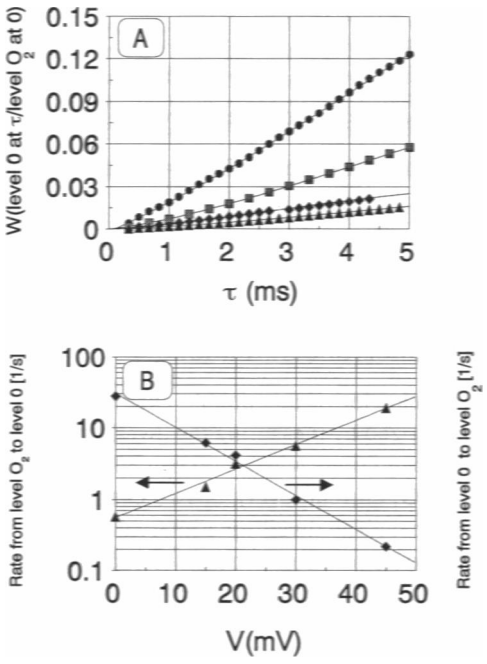

FIGURE 6 Voltage dependence of the transition rates between current levels 0 and O_2. (*A*) Example of a conditional probability analysis. The time dependence of the conditional probability *W*(level 0,τ/level O_2,0) was measured from current traces recorded at 0 (▲), 15 (◆), 30 (■), and 45 mV (●) as a function of τ. The continuous lines were obtained by curve fitting to a polynomial function of the form $\alpha_1\tau + \alpha_2\tau^2 + \alpha_3\tau^3$, the time dependence of the conditional probability estimated at various potentials. The transition rate from current level O_2 to level 0 at each potential was given by α_1. (*B*) Logarithmic representation of the voltage dependence of the transition rates between the current levels 0 and O_2. The continuous lines represent simple exponential functions with, respectively, an *e*-fold increase in the transition rate from level O_2 to level 0/12.7 mV, and an *e*-fold decrease in the transition rate from level 0 to level O_2/9 mV. These results were obtained from current records filtered at 5 kHz and sampled at 30 kHz.

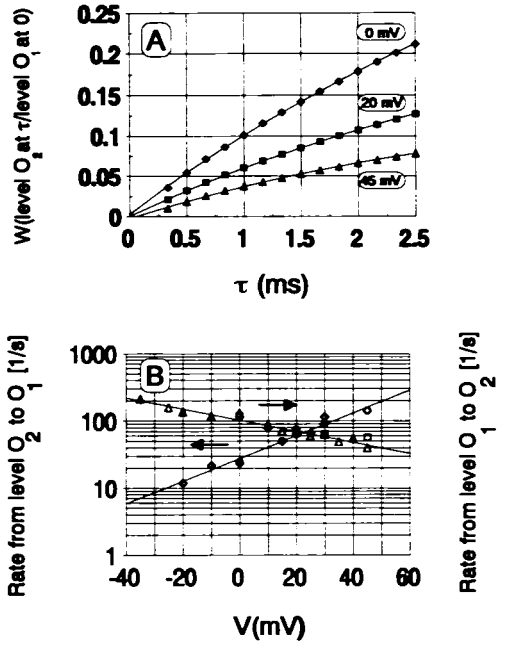

FIGURE 7 Voltage dependence of the transition rates between the current levels O_1 and O_2. (*A*) Example of a conditional probability analysis. The continuous lines were obtained by curve fitting to a polynomial function of the form $a_1\tau + a_2\tau^2 + a_3\tau^3$ the time dependence of the conditional probability estimated at various potentials. The linear coefficient a_1 provided a direct measurement of the transition rate between the current levels O_1 and O_2. (*B*) Logarithmic representation of the voltage dependence of the transition rates between the current levels O_1 and O_2 measured using either the conditional procedure shown in *A* (○ and □), or the eight-state HMM approach described previously (◇ and △). The continuous lines correspond to single exponential functions with an *e*-fold increase/26.2 mV for the transition rate from O_2 to O_1 and an *e*-fold decrease/52 mV for the transition rate from O_1 to O_2. These results were obtained from current records filtered at 5 kHz and sampled at 30 kHz.

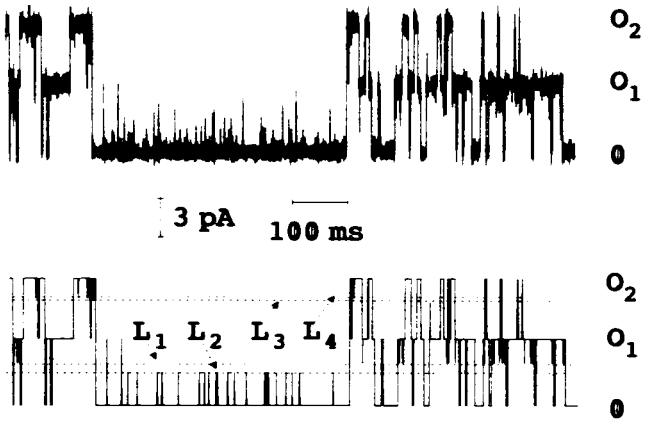

FIGURE 8 Noise-free current records resulting from the application of the Baum-Welch reestimation formulae on current traces obtained experimentally. *Top*: Original signal at 25 mV sampled at 3 kHz and filtered at 1 kHz. The Hidden Markov analysis was carried out on segments of 200,000 samples and included seven adjustable current levels. The seven current levels are apparent in the record shown in the bottom panel. Three of these levels marked O_1, O_2, and 0 had a significant degree of occurrence. The intermediate current levels L_1, L_2, L_3, and L_4 were added to take into account fast transitions between O_1 and 0 or between O_2 and O_1. The probability of occurrence of each of these levels was less than 0.01, and their contribution affected minimally the estimation of P_o. The 50% reference levels used to detect the transitions 0–O_1 or O_1–O_2 were taken as the mean values of L_1 and L_2 or L_3 and L_4.

analysis is presented in Fig. 8. Despite the fact that seven independent current levels were initially included, the HMM analysis indicated that three levels only, namely levels 0 (states S_0 and S^1_0), O_1 (state S_{O_1}), and O_2 (state S_{O_2}), were characterized by probabilities of occurrence greater than 0.01. These current levels refer specifically to the binomial channel system described previously with, respectively, no monomer, one monomer, or two monomers open. The occurrence of the intermediate current levels L_1, L_2, L_3, and L_4 represented less than 1% of the total channel activity, thus precluding any significant contribution to the current amplitude histograms shown in Fig. 2. The transition rates to the intermediate current levels L_1, L_2, L_3, and L_4 were not therefore included in the present analysis, a procedure that allowed a selective omission of the kinetic states with negligible mean dwell times (<0.3 ms).

The results in Fig. 7 *B* show that the HMM technique and the conditional probability approach led to nearly identical rate constant values. Fig. 7 *B* demonstrates also that the transition rates from level O_1 to O_2 and from level O_2 to O_1 can be expressed in terms of monoexponential functions. The continuous lines were computed according to:

$$\text{Rate from level } O_1 \text{ to level } O_2 = 105e^{[-0.49\ qV/KT]} \quad (12)$$

and

$$\text{Rate from level } O_2 \text{ to level } O_1 = 27e^{[0.95\ qV/KT]} \quad (13)$$

Dwell time interval distributions

The kinetic behavior of this double channel system was finally characterized by measuring the dwell time interval distributions in conditions where no channel (0 current level), one channel (O_1 current level), or two channels (O_2 current level) were open. The dwell time interval analysis was carried out according to the method described by Sigworth and Sine (1987) on nonsegmented current records (silent periods between the current bursts included). Time intervals were measured on noise-free signals resulting from the application of the Baum-Welch reestimation formulae on current traces obtained experimentally, as illustrated in Fig. 8. Transitions were measured using threshold current values TH_1 and TH_2 taken as the mean values of L_2, L_1 and L_3, L_4. The resulting time interval distributions for current levels O_1, O_2, and 0 are presented in Figs. 9, 10, and 11, respectively. Clearly, the time interval distributions measured at all potentials for currents at levels O_1 and O_2 were well fitted by single exponential functions for time intervals ranging from 1 ms to 1 s. The dwell time distribution for currents in O_1 did not vary in a significant manner as a function of voltage with mean

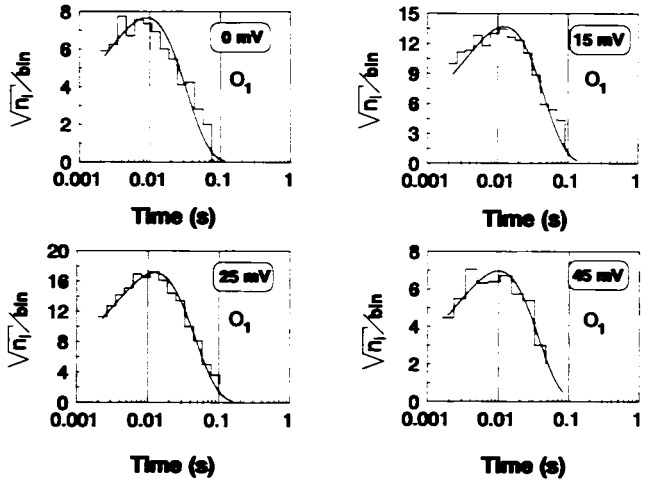

FIGURE 9 Open time interval distributions in conditions where one channel was open (O_1 current level). Distributions were plotted with a logarithmic time axis. n_i represents the number of intervals/bin. Except for the histogram at +45 mV, which was obtained from 700 intervals, the remaining histograms were computed from a minimum of 3400 intervals. Each dwell time distribution could be fitted by a single exponential function for time interval ranging from 1 to 100 ms. The histograms were obtained on noise-free current records derived from current records sampled at 5 kHz and filtered at 1 kHz.

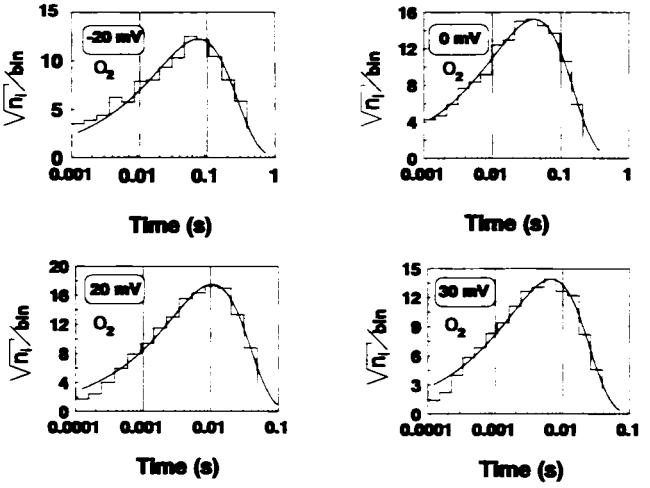

FIGURE 10 Open time interval distributions in conditions where two channels were open (O_2 current level). Distributions were plotted with a logarithmic time axis. Histograms were computed from a minimum of 3000 intervals. Each dwell time distribution could be fitted by a single exponential function for time interval ranging from 1 ms to 1 s. Experimental conditions as in Fig. 9.

values equal to 8.9, 12.1, 12.6, and 9.9 ms for holding potentials of 0, 15, 25, and 45 mV, respectively. However, the mean dwell time for currents in O_2 showed a strong voltage dependence with values of 74.0, 41.6, 15, and 8.8 ms for membrane potentials equal to −20, 0, 20, and 30 mV, respectively. Two exponential functions were required to describe the dwell time distribution for currents in level 0. The time constant of the fast exponential did not change appreciably as a function of voltage, whereas the second exponential coming from the silent periods between bursts of channel activity appeared strongly voltage-dependent.

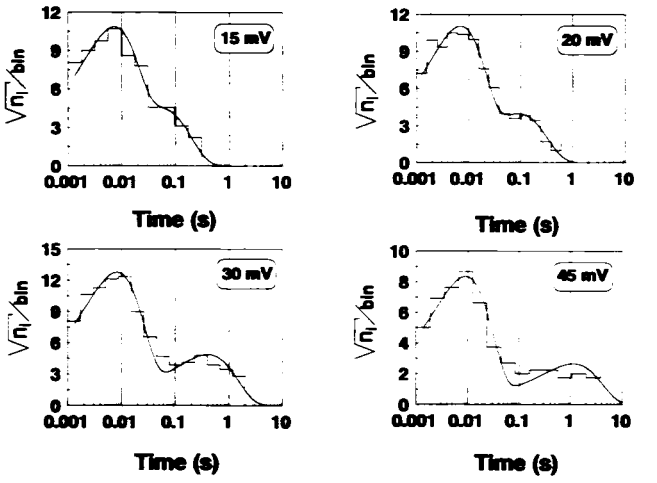

FIGURE 11 Closed time interval distributions. Distributions were plotted with a logarithmic time axis. Histograms were computed from a minimum of 500 intervals. The dwell time distributions were fitted by a summation of two exponential functions for time intervals ranging from 1 ms to 10 s. Experimental conditions as in Fig. 9.

Kinetic model analysis

The results presented in the previous analysis provide the proper background to enable a discrimination of the kinetic models that have the potential to account for the fluctuation patterns illustrated in Fig. 1. To be valid, the proposed model must take into consideration 1) that the observed channel system behaves as two independent monomeric channels of identical conductance within bursts of channel activity; 2) that there are direct transitions between the current levels O_2 and 0; and, finally, 3) that the dwell time distributions of the current in levels O_1 and O_2 correspond to monoexponential functions, whereas a minimum of two exponentials is needed to describe correctly the distribution of the time intervals in level 0.

A model compatible with these requirements was considered by Miller (1982) in a single channel analysis of the Cl^- selective channel from the *T. californica* electroplax membrane. The proposed kinetic scheme contains four different states with two nonconducting states (S_0 and S_1 in scheme 1):

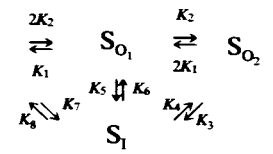

Scheme 1

In this model, the channel is viewed essentially as two independent subunits of identical conductance that are

coupled through a common inactivated state S_1. The states along the top row in scheme 1 describe the kinetic behavior resulting from the superposition of the two monomeric channels with each monomer fluctuating according to the identical two-state Open-Closed kinetic (scheme 2).

$$C \underset{K_1}{\overset{K_2}{\rightleftarrows}} O$$

Scheme 2

The overall scheme would be compatible with the observation that the dwell time distributions for current in levels O_2 and O_1 need to result in single exponential functions. Within this framework, the labels S_0, S_{O_1}, S_{O_2} in scheme 1 refer to states with, respectively, no channel (CC), one channel (OC), or two channels (OO) open at the same time. A key feature of this model consists of a common inactivated state that is accessible in conditions where there are no channel, one channel, or two channels open. The observed direct transitions between current levels O_2 and 0 represent, therefore, the particular case of transitions between states S_1 and S_{O_2}. Finally, it should be stressed that, because of microreversibility, the transition rates in scheme 1 are not independent but are related according to $2K_1 K_5 K_4 = K_2 K_3 K_6$ and $2K_2 K_5 K_8 = K_1 K_7 K_6$. Several parameters can now be computed on the basis of this model:

1) the open probability of a single monomeric channel defined as

$$P_o = \frac{2P(O_2)}{2P(O_2) + P(O_1)} = \frac{K_2}{K_2 + K_1} \quad (14)$$

where $P(O_1)$ and $P(O_2)$ are the probabilities of occurrence of current levels O_1 and O_2, respectively.

2) the open probability of the slow gate defined as

$$P_{gate} = \frac{P(O_2)}{P_o^2} = 1 \Big/ \left(1 + \frac{K_3}{K_4}\left[\frac{K_2}{K_2 + K_1}\right]^2\right) \quad (15)$$

3) the ratio probability of occurrence of level 0 over the probability of occurrence of current level O_1

$$\frac{P(\text{level } 0)}{P(O_1)} = \frac{1}{2}\left[\frac{K_1}{K_2} + \frac{K_3 K_2}{K_4 K_1}\right] \quad (16)$$

where P (level 0) is the probability of occurrence of current level 0. The expression for P (level 0) is obtained by summing the probabilities of the closed states S_C and S_1.

These parameters are model-independent and can readily be computed from the current amplitude histograms derived from individual current records. The validity of the model presented in scheme 1 was tested by comparing the experimental values obtained for each of these parameters at various potentials with the predictions of Eqs. 14, 15, and 16, using the expressions 10, 11, 12, and 13 for the rate constants K_1, K_2, K_3, and K_4, namely:

$$K_3 = \text{Rate from level } O_2 \text{ to level } 0 = 0.55e^{[1.97\,qV/KT]} \quad (17)$$

$$K_4 = \text{Rate from level 0 to level } O_2 = 29e^{[-2.74\,qV/KT]} \quad (18)$$

$$K_2 = \text{Rate from level } O_1 \text{ to level } O_2 = 105e^{[-0.49\,qV/KT]} \quad (19)$$

and

$$2K_1 = \text{Rate from level } O_2 \text{ to level } O_1 = 27e^{[0.95\,qV/KT]} \quad (20)$$

The variation of P_o, the monomeric channel open probability, as a function of the applied voltage is illustrated in Fig. 12. The continuous line is the prediction of Eq. 14 with K_2 and K_1 computed according to Eqs. 19 and 20. The open circles correspond to the experimental values of P_o derived from $P(O_1)$ and $P(O_2)$ according to Eq. 14. The filled squares and the + symbols represent the values of P_o calculated from Eq. 2 on current records where interburst silent periods were omitted (see Fig. 4). The agreement between the experimental and theoretical values confirms that Eq. 14, with K_2 and K_1 given by Eqs. 19 and 20, accounts for the voltage dependence of P_o. In addition, the fact that the experimental values of P_o obtained from Eq. 14 on current records, which included silent interburst periods, agreed with the values of P_o computed from Eq. 2 using current amplitude histograms measured exclusively within bursts of channel activity, provides further support to the proposal of a binomial kinetic scheme relating states S_C, S_{O_1}, and S_{O_2}. The voltage dependence of the slow gate open probability P_{gate} is shown in Fig. 13 *A*. Curve 1 is the prediction of Eq. 15 with K_3, K_4, K_2, and K_1 given by Eqs. 17, 18, 19, and 20. A significant agreement was obtained between the experimental data and the predicted values over the entire voltage range. On the basis of this result it appears that the single channel activity shown in Fig. 1 is compatible with a model in which two monomeric channels have access to a common inactivated state. This conclusion was further supported by results coming from an analysis of the voltage dependence of P_{ratio}, the ratio probability of occurrence of level 0 over the probability of occurrence of current level O_1. A comparison between the theoretical predictions based on Eq. 16 (curve 1) and the

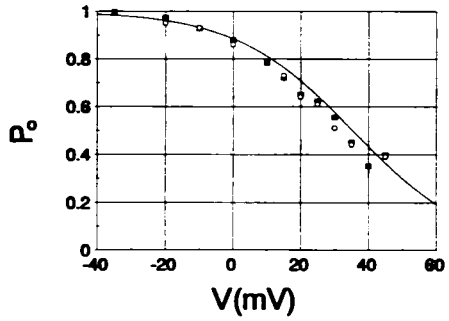

FIGURE 12 Variation of P_o as a function of the applied voltage. (○) values of P_o derived from Eq. 14 using $P(O_1)$ and $P(O_2)$ computed from current records that included silent interburst periods. (■, +) values of P_o computed from two different experiments using Eq. 2 and values of $P(O_1)$ and $P(O_2)$ derived from current amplitude histograms measured on current records where interburst silent periods were omitted. The continuous line is the prediction of Eq. 14 with K_2 and K_1 computed according to Eqs. 19 and 20.

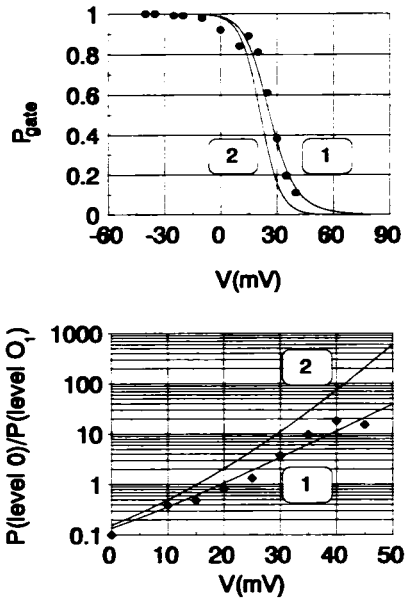

FIGURE 13 (*A*) Variation of the parameter P_{gate} as a function of voltage. Curve 1 was computed from Eq. 15 and represents the prediction of the single-inactivated state model illustrated in scheme 1. Curve 2 represents the prediction of the main-gate model shown in scheme 3. (*B*) Voltage dependence of the ratio probability of level 0 over probability of level O_1. The theoretical curve 1 was computed from Eq. 16 derived for the single-inactivated state model. Curve 2 is the prediction of the main-gate model (see scheme 3). The voltage dependence of the rate constants K_1, K_2, K_3, and K_4 was computed according to Eqs. 20, 19, 17 and 18, respectively.

experimental estimations of P_{ratio} at various potentials is presented in Fig. 13 *B*. There is again a clear agreement between curve 1 and the experimental values of P_{ratio} over the entire voltage range. This final result provides strong evidence that the model shown in scheme 1, which included a single inactivated state, accounts for the main statistical features of the single channel activity illustrated in Fig. 1.

Double-barreled channels can be also modeled using kinetic schemes such as the one proposed by Hunter and Giebisch (1987) to describe a potassium-selective channel in renal tubules.

$$\begin{array}{ccccc} S_C & \overset{2K_2}{\rightleftarrows} & S_{O_1} & \overset{K_2}{\rightleftarrows} & S_{O_2} \\ K_3 \uparrow\downarrow K_4 & \overset{K_1}{} & K_3 \uparrow\downarrow K_4 & \overset{2K_1}{} & K_3 \uparrow\downarrow K_4 \\ S^c_C & \overset{2K_2}{\rightleftarrows} & S^c_{O_1} & \overset{K_2}{\rightleftarrows} & S^c_{O_2} \\ & \underset{K_1}{} & & \underset{2K_1}{} & \end{array} \qquad \begin{array}{l} \text{Main Gate open} \\ \\ \text{Main Gate closed} \end{array}$$

Scheme 3

According to this model, the channel consists of a system of two independent monomeric channels with a common main gate. The latter can open or close independently of the state of the two-monomeric channel system. It is assumed again that each monomer fluctuates according to the two-state model presented in scheme 2. The states S^c_0, $S^c_{O_1}$ and $S^c_{O_2}$ (see scheme 3) are considered nonconducting because of the closure of the main gate, but the two monomeric channels are presumed still to fluctuate independently despite closure of the gate. In conditions where the main gate is open, however, the entire system behaves as two independent channels as observed in bursts of channel activity. Finally, the direct transitions between current levels O_2 and O observed experimentally correspond in this case to the closures or openings of the main gate while the two monomeric channels are open (S_{O_2} state). It can be shown that this model predicts a voltage dependence for P_o identical to the one expressed in Eq. 14. Therefore, the results in Fig. 12 cannot be used to invalidate one of two models proposed so far. The voltage dependence of P_{gate} predicted by the main-gate model is illustrated as curve 2 in Fig. 13 *A*. Despite a good agreement between the predicted (curve 2) and experimental values at negative potentials, this model failed to account for the voltage dependence of P_{gate} at more positive potential values. A more important discrepancy between the experimental data and the predictions of the main-gate model resulted also from an analysis of P_{ratio}. Curve 2 in Fig. 13 *B* illustrates the predicted variation of P_{ratio} as a function of voltage. Clearly, this model overestimated the value of P_{ratio} at positive potentials. These observations suggest, therefore, that a model consisting of two monomeric channels coupled to an independent main gate cannot completely account for the statistical characteristics of the current fluctuations presented in Fig. 1.

Finally, a correlation analysis led to the proposal by Labarca et al. (1985) of a modified version of the model suggested by Miller (1982) for the *T. californica* Cl^- channel. The channel would still be formed of two parallel subunits of identical conductance and kinetics, but the states S_C and S_{O_2} would now be connected via two parallel states, namely S_{O_1} and $S^*_{O_1}$. In addition, only state S_C would have access to the inactivated state S_1. Because this model does not include direct transitions between current levels O_2 and O, it cannot be compatible with the present findings. Furthermore, Eq. 9 leads in this case to a conditional probability W (level O at τ/level O_2 at 0) of the form $\alpha_3\tau^3 + \alpha_4\tau^4 + \cdots$ which cannot account for the time dependence of the conditional probability data shown in Fig. 6 *A*. However, the model suggested by Miller (1982) is far from being unique, and the results presented in Figs. 12 and 13 are certainly compatible with an ensemble of models having kinetic features more complex than the one presented here. In addition it must also be stressed that the time interval analysis that was carried out did not include states with low probability of occurrence. A more realistic model should include those additional low-occurrence states.

DISCUSSION

The present work has provided evidence for a double-barreled Cl^- selective channel of 160 pS in SRER microsomes isolated from rat hepatocytes. On the basis of a detailed single channel statistical analysis, it was concluded that the voltage dependence of the channel open probability arises from two main gating mechanisms: 1) a binomial

gating process that controls the openings of two independent monomeric channels, and 2) a slow gating process that accounts for the voltage-dependent inactivation of this double monomeric channel system. It was also shown that a model in which two monomeric channels have access to a single inactivated state provides a better description of the statistical properties of this double-barreled anionic channel than a model involving two monomeric channels coupled to a main gate.

Predicted mean current voltage dependence

The hypothesis that the current levels 0, O_1, and O_2 are distributed according to a binomial distribution within individual current burst was confirmed through a χ^2 analysis based on a limited number of independent observations. The requirement of a small number (500) of independent current values was essential to ensure the applicability of the χ^2 test and demonstrate that the observed deviations from the binomial distribution were within the expected errors related to the stochastic nature of the current fluctuations. As a result of the binomial distribution of the current levels, the probability of the slow gate can now be expressed as

$$P_{gate} = \frac{P(O_2)}{P_o^2} = \frac{P(O_1)}{2P_o(1 - P_o)} \quad (21)$$

It follows from this equation that the mean current $\langle I \rangle$ defined as

$$\langle I \rangle = 2\Delta I P(O_2) + \Delta I P(O_1) \quad (22)$$

where ΔI, the unitary current amplitude at a given potential, can now be written as

$$\langle I \rangle = 2\Delta I P_o P_{gate} \quad (23)$$

Because both P_o and P_{gate} were found to decrease at positive potentials, the mean number of open channel, $\langle I \rangle/\Delta I$, is not expected to display a bell-shaped voltage dependence. The channel reported in this work differs, therefore, substantially from the anionic channel of large conductance (260 pS) observed in giant liposomes made from rat pancreas ER vesicles (Schmid et al., 1988) or from the well characterized voltage-dependent anionic channel VDAC (Colombini, 1983; Tedeschi et al., 1987). Moreover, none of the channels identified so far in ER preparations showed clear double-barreled-like properties compatible with the results presented in this study. Finally, despite the observations that many of the channels identified in intracellular membrane preparations such as the mitochondrial external membrane (Colombini, 1983; Tedeschi et al., 1987), endosomal vesicles (Schmid et al., 1989), or lysosomal membranes (Tilly et al., 1992) showed multiple conductance levels, there is no indication of double-barreled-like features in these cases.

Comparison with double-barreled channels found in other preparations

The presence of double-barreled Cl^- channels has been reported in at least three different membrane preparations. The most detailed single channel characterization was provided by Miller and co-workers who carried out an extensive study of a double-barreled chloride channel obtained by fusion of vesicles from the electroplax surface membrane of *T. californica* into a planar bilayer (White and Miller, 1981; Miller, 1982; Hanke and Miller, 1983; Miller and White, 1984: see also Tank et al., 1982). The unitary conductance of this channel was estimated at 9 pS in 140 mM KCl, and the channel was found to be highly selective for Cl^- ions. Two distinct voltage-dependent processes were identified: a slow voltage-dependent gating process that would maintain the channel in an inactivated state at positive potentials (*cis* relative to *trans*), and a binomial gating of single channels with an open probability decreasing at negative potential values (*cis* relative to *trans*). Assuming that these two mechanisms work independently, the voltage dependence of the macroscopic conductance would then correspond to a bell-shaped curve centered around −50 mV. This channel has been expression-cloned in oocytes, indicating that a single polypeptide either alone or in homooligomeric complex is sufficient to give rise to all the biophysical properties of the *Torpedo* channel (Bauer et al., 1991). More recently, the purification and functional reconstitution of this channel had led to the conclusion that the *Torpedo* double-barreled channel is most likely constructed as a homodimer (Middleton et al., 1994). Despite a similar fluctuation pattern, there are nevertheless important differences between the *Torpedo* Cl^- channel and the double-barreled channel described in this work. First, the Cl^- channel from the electroplax membrane has a single channel conductance substantially smaller than that estimated for the Cl^- channel obtained from SRER microsomes. However, the extent of this difference cannot be clearly assessed because the dependence of the single channel conductance of the rough reticulum channel as a function of the Cl^- concentration is not currently known. Secondly, the voltage dependence curves of the slow and binomial gating precesses are inverted in the case of the *Torpedo* channel, whereas the results presented in Figs. 12 and 13 *A* show clearly that both P_o and P_{gate} increase at negative potential values. This observation rules out the possibility that the voltage dependence of the 160-pS channel corresponds to that of a *Torpedo* channel inserted differently in the bilayer. In addition, the binomial gating process of the 160-pS channel showed a greater voltage sensitivity with a 26.2-mV change in transmembrane potential for an *e*-fold variation in the rate of channel closure K_1 (see Fig. 7 *B*), compared with the 50-mV change needed to produce a similar variation in the rate of channel closure for the *Torpedo* channel. The main difference between our results and the observations reported for the *Torpedo* channel concerns, however, the slow gating process. For instance, the results in Fig. 13 *A* show that P_{gate} increases when the potential applied in the *cis* compartment is more positive relative to *trans*. In contrast, the probability of burst formation for the *Torpedo* channel decreases under identical voltage conditions (Miller and Richard, 1990). These results suggest, therefore, that there are important differences between these two Cl^- permeable double-barreled channels with regard to

the magnitude and polarity of the effective charge responsible for the slow gating process.

Double-barreled chloride channels were also observed in a series of patch clamp experiments in distal rabbit nephron (Sansom et al., 1990) and in vesicles obtained from the apical membrane of shark rectal gland (SRG) (La et al., 1991). The monomeric channel conductance was estimated at 23 pS (140 mM KCl) in rabbit distal nephron and 62 pS (300/50 mM KCl) in SRG. In each of these studies, the open probability of the subchannel increased at hyperpolarizing cell potentials. To be compatible with the present findings the *trans* chamber in our case has to correspond to the cell side. Within this framework, the polarity of the voltage dependence of the substate open probability would be in agreement with the results reported in Fig. 12. However, as for the *Torpedo* Cl^- channel, the voltage sensitivity of P_o shown in Fig. 12 appears significantly more important than that found for the Cl^- channels of the cortical collecting duct and SRG. Moreover, the unitary conductance is markedly larger in the case of the SRER channel and the P_{gate} versus voltage relationship in Fig. 13 *A* is inverted compared with the double-barreled Cl^- channel reported in these preparations.

Physiological role of the 160-pS double-barreled Cl^- channel

Several studies have established that the uptake of Ca^{2+} in RER is dependent on the presence of monovalent cations and anions (see, e.g., Bayerdörffer et al., 1984). It was proposed, for instance, that the Ca^{2+}-ATPase activity in RER vesicles is coupled to a passive movement of anions to insure electroneutrality (Kemmer et al., 1987). This hypothesis gained further support when the presence of anion-permeable channels was confirmed in liposomes made of ER vesicles from rat pancreas (Schmid et al., 1988). However, as discussed, these channels showed a voltage dependence and single channel unitary conductances different from the 160-pS channel reported in this work. It was also postulated that Cl^- selective channels could be involved in the maintenance of electroneutrality during H^+ uptake into endocytotic vesicles (Schmid et al., 1989). However, the Cl^- channels identified in endosomal vesicles from rat kidney cortex did not display double-barreled-like features. Moreover, a contribution of the 160-pS channel to a Ca^{2+} or H^+ uptake process remains unlikely because of the voltage dependence of the channel gating mechanisms. The Cl^- channel reported in this work showed an increased open probability at negative potentials (*trans* relative to *cis*). Most of the vesicles used for channel incorporation are presumed to be oriented right side out with the vesicle internal milieu corresponding to the luminal compartment of the ER. The cytoplasmic domain of the channel should therefore be in contact with the *cis* solution (Paiement and Bergeron, 1983). Under these conditions, a negative potential inside the ER (*trans*) relative to the cytosol (*cis*) should lead to channel activation and Cl^- ion fluxes. The extent of the membrane potential variations inside the ER during Ca^{2+} release is currently unknown. Within the proposed framework, however, the presence of negative charges inside the ER resulting, e.g., from an efflux of Ca^{2+} ions, may lead to the activation of the 160-pS Cl^- channel. It is thus possible that the channel identified is part of an ensemble of ionic pathways at the ER level responsible for electroneutrality and/or luminal ER potential control.

CONCLUSION

We have shown the presence of a Cl^- channel in SRER microsomes, a fraction highly enriched in ER membranes. The gating mechanism of this novel double-barreled Cl^- channel of large unitary conductance was investigated at the single channel level. Our analysis provided clear evidence that the open channel probability is controlled in this case by at least two gating processes working independently. However, a more detailed investigation of the pharmacological properties and control mechanisms of this channel will be required to confirm its contribution to a counter-ion movement during the release and/or uptake of Ca^{2+} and H^+ ions in intracellular stores.

APPENDIX 1

Let us consider the following kinetic scheme:

$$C \underset{K_1}{\overset{2K_2}{\rightleftarrows}} O_1 \underset{2K_1}{\overset{K_2}{\rightleftarrows}} O_2$$

Scheme 4

which would lead to three distinct current levels, namely: level C, level O_1, and level O_2. The solution of the Kolmogorov forward equation yields in this case:

$$W(\text{level C}, \tau/\text{level O}_2, 0) = \left[\frac{K_1}{K_1 + K_2}\right]^2 [1 - e^{-(K_1+K_2)\tau}]^2 \tag{24}$$

For $\tau \to 0$ the Eq. 24 now reads:

$$W(\text{level C}, \tau/\text{level O}_2, 0) \to K_1^2\tau^2 \tag{25}$$

The power expension of the conditional probability W(level C, τ/level O_2, 0) does not contain in this case a linear term in τ, since direct transition from current level O_2 to level C cannot occur without transitions to an intermediate current level (O_1 level). However, the conditional probability W(level C, τ/level O_1, 0) namely:

$$W(\text{level C}, \tau/\text{level O}_1, 0) = \frac{K_1 e^{-2(K_1+K_2)\tau}[-1 + e^{(K_1-K_2)\tau}][K_1 e^{(K_1+K_2)\tau} + K_2]}{(K_1 + K_2)^2} \tag{26}$$

will become as $\tau \to 0$ approximately equal to

$$W(\text{level C}, \tau/\text{level O}_1, 0) \cong K_1\tau - K_1(2K_2 + K_1)\tau^2 + \cdots \tag{27}$$

In this case, the power expansion of W(level C, τ/level O_1, 0) contains a linear term, an indication that direct transitions from levels O_1 and C can take place without transitions to an intermediate current level. It must be mentioned that Eqs. 25 and 27 could have been as well derived using Eq. 9. In addition, Eq. 27 shows that an estimation of the rate of transition K_1 follows directly from the linear coefficient $K_1\tau$. Finally, the approximated formulae in Eqs. 25 and 27 should remain valid as long as τ is small compared with $1/(K_1 + K_2)$, the characteristic correlation time between levels C and O_1.

The authors would like to thank Dr. Jacques Paiement and Mrs. Line Roy for all of their advice concerning the preparation and fusogenic properties

of rough endoplasmic reticulum microsomes. Rémy Sauvé is a senior fellow from the Fonds de la Recherche en Santé du Québec.
This work was supported by a grant from the Medical Research Council of Canada.

REFERENCES

Bauer, C. K., K. Steinmeyer, J. R. Schwarz, and T. J. Jentsch. 1991. Completely functional double-barreled chloride channel expressed from a single *Torpedo* cDNA. *Proc. Natl. Acad. Sci. USA.* 88: 11052–11056.

Bayerdörffer, E., H. Streb, L. Eckhardt, W. Haase, and I. Schulz. 1984. Characterization of calcium uptake into rough endoplasmic reticulum of rat pancreas. *J. Membr. Biol.* 81:69–82.

Chung, S. H., J. B. Moore, L. Xia, L. S. Premkumar, and P. W. Gage. 1990. Characterization of single channel currents using digital signal processing based on Hidden Markov Models. *Philos. Trans. R. Soc. Lond. B. Biol. Sci.* 329:265–285.

Colombini, M. 1983. Purification of VDAC (voltage-dependent anion-selective channel) from rat liver mitochondria. *J. Membr. Biol.* 74: 115–121.

Hals, G. D., P. Stein, and P. T. Palade. 1989. Single channel characteristics of a high conductance anion channel in "sarcoballs". *J. Gen. Physiol.* 93:385–410.

Hanke, W., and C. Miller. 1983. Single chloride channels from *Torpedo* electroplax. Activation by protons. *J. Gen. Physiol.* 82:25–45.

Hunter, M., and G. Giebisch. 1987. Multi-barrelled K channels in renal tubules. *Nature* 327:522–524.

Keller, B. U., J. Kleineke, M. Criado, and H. D. Söling. 1988. Single channel recordings from endoplasmic reticulum membranes of rat liver: a patch clamp study on giant vesicles. *Pflügers Arch.* 411:R105.

Kemmer, T. P., E. Bayerdörffer, H. Will, and I. Schulz. 1987. Anion dependence of Ca^{2+} transport and (Ca^{2+} + K^+)-stimulated Mg^{2+}-dependent transport ATPase in rat pancreatic endoplasmic reticulum. *J. Biol. Chem.* 262:13758–13764.

La, B. Q., S. L. Carosi, J. D. Valentich, S. Shenolikar, and S. C. Sansom. 1991. Regulation of epithelial chloride channels by protein phosphatase. *Am. J. Physiol.* 260:C1217–C1223.

Labarca, P., J. A. Rice, D. R. Fredkin, and M. Montal. 1985. Kinetic analysis of channel gating. Application to the cholinergic receptor channel and the chloride channel from *Torpedo californica*. *Biophys. J.* 47:469–478.

Middleton, R. E., D. J. Pheasant, and C. Miller. 1994. Purification and functional reconstitution of a voltage gated channel from *Torpedo* electrical organ *Biophys. J.* 66:A142.

Miller, C. 1982. Open-state substructure of single chloride channels from *Torpedo* electroplax. *Philos. Trans. R. Soc. Lond. B. Biol. Sci.* 299: 401–411.

Miller, C., and E. A. Richard. 1990. The voltage-dependent chloride channel of the *Torpedo* electroplax: intimations of molecular structure from quirks of single-channel function. *In* Chloride Channels and Carriers in Nerve, Muscle and Glial Cells. F. J. Alvarez-Leefmans and J. M. Russell, editors. Plenum Press, New York. 383–405.

Miller, C., and M. M. White. 1984. Dimeric structure of single chloride channels from *Torpedo* electroplax. *Proc. Natl. Acad. Sci. USA.* 81: 2772–2775.

Morier, N., and R. Sauvé. 1993. Double-barrelled Cl^- channel of large conductance in rough endoplasmic reticulum membrane from rat hepatocytes. *Biophys. J.* 64:A380.

Muallem, S., M. Schoeffield, S. Pandol, and G. Sachs. 1985. Inositol trisphosphate modification of ion transport in rough endoplasmic reticulum. *Proc. Natl. Acad. Sci. USA.* 82:4433–4437.

Murray, D. and R. Ashley. 1991. An intracellular anion channel from rat brain microsomes which is also permeable to cations. *Biochem. Soc. Trans.* 19:255S.

Paiement, J., and J. J. Bergeron. 1983. Localization of GTP-stimulated core glycosylation to fused microsomes. *J. Cell Biol.* 96:1791–1796.

Paiement, J., F. W. Kan, J. Lanoix, and M. Blain. 1988. Cytochemical analysis of the reconstitution of endoplasmic reticulum after microinjection of rat liver microsomes into *Xenopus* oocytes. *J. Histochem. Cytochem.* 36:1263–1273.

Paiement, J., D. Rindress, C. E. Smith, L. Poliquin, and J. J. Bergeron. 1987. Properties of a GTP sensitive microdomain in rough microsomes. *Biochim. Biophys. Acta.* 898:6–22.

Palade P., C. Dettbarn, P. Volpe, B. Alderson, and A. S. Otero. 1989. Direct inhibition of inositol-1,4,5-trisphosphate-induced Ca^{2+} release from brain microsomes by K^+ channel blockers. *Mol. Pharmacol.* 36:664–672.

Rousseau, E. 1989. Single chloride-selective channel from cardiac sarcoplasmic reticulum studied in planar lipid bilayers. *J. Membr. Biol.* 110:39–47.

Rousseau, E., M. Roberson, and G. Meissner. 1988. Properties of single chloride selective channel from sarcoplasmic reticulum. *Eur. Biophys. J.* 16:143–151.

Sansom, S. C., B. Q. La, and S. L. Carosi. 1990. Double-barreled chloride channels of collecting duct basolateral membrane. *Am. J. Physiol.* 258: F46–F52.

Sauvé, R., C. Simoneau, R. Monette, and G. Roy. 1986. Single-channel analysis of the potassium permeability in HeLa cancer cells: evidence for a calcium-activated potassium channel of small conductance. *J. Membr. Biol.* 92:269–282.

Sauvé, R., G. Roy, and D. Payet. 1983. Single channel K^+ currents from HeLa cells. *J. Membr. Biol.* 74:41–49.

Schmid, A., H. Gögelein, T. P. Kemmer, and I. Schulz. 1988. Anion channels in giant liposomes made from endoplasmic reticulum vesicles from rat exocrine pancreas. *J. Membr. Biol.* 104:275–282.

Schmid, A., G. Burckhardt, and H. Gögelein. 1989. Single chloride channels in endosomal vesicle preparations from rat kidney cortex. *J. Membr. Biol.* 111:265–275.

Shah, J., R. S. Cohen, and H. C. Pant. 1987. Inositol trisphosphate-induced calcium release in brain microsomes. *Brain Res.* 419:1–6.

Shah, J., and H. C. Pant. 1988. Potassium-channel blockers inhibit inositol trisphosphate-induced calcium release in the microsomal fractions isolated from the rat brain. *Biochem. J.* 250:617–620.

Simon, S. M., G. Blobel, and J. Zimmerberg. 1989. Large aqueous channels in membrane vesicles derived from the rough endoplasmic reticulum of canine pancreas or the plasma membrane of *Escherichia coli*. *Proc. Natl. Acad. Sci. USA.* 86:6176–6180.

Sigworth, F. J., and S. M. Sine. 1987. Data transformations for improved display and fitting of single-channel dwell time histograms. *Biophys. J.* 52:1047–1054.

Tanifuji, M., M. Sokabe, and M. Kasai. 1987. An anion channel of sarcoplasmic reticulum incorporated into planar lipid bilayers: single-channel behavior and conductance properties. *J. Membr. Biol.* 99:103–111.

Tank, D. W., C. Miller, and W. W. Webb. 1982. Isolated-patch recording from liposomes containing functionally reconstituted chloride channels from *Torpedo* electroplax. *Proc. Natl. Acad. Sci. USA.* 79:7749–7753.

Tedeschi, H., C. A. Mannella, C. L. Bowman. 1987. Patch clamping the outer mitochondrial membrane. *J. Membr. Biol.* 97:21–29.

Tilly, B. C., G. M. Mancini, J. Bijman, P. G. van Gageldonk, C. E. Beereas, R. J. Bridges, H. R. de Jonge, and F. W. Verheijen. 1992. Nucleotide-activated chloride channels in lysosomal membranes. *Biochem. Biophys. Res. Commun.* 187:254–260.

White, M. M., and C. Miller. 1981. Chloride permeability of membrane vesicles isolated from *Torpedo* electroplax. *Biophys. J.* 35:455–462.